Tampere University

Jadon Stuart

EFFECT OF INTERFACIAL SiO_2 ON PERFORMANCE OF RUTILE TiO_2/Si PHOTOANODES FOR SOLAR FUEL PRODUCTION

Bachelor of Science Thesis
Faculty of Engineering and Natural Sciences
Examiner: Prof. Mika Valden
April 2023

ABSTRACT

Jadon Stuart: Effect of Interfacial SiO_2 on Performance of Rutile TiO_2/Si Photoanodes for Solar Fuel Production
Bachelor of Science Thesis
Tampere University
Science and Engineering Degree Program
April 2023

Photoelectrochemical cells have the potential to revolutionize clean hydrogen production by harnessing solar power and carrying out water-splitting reactions. This thesis considers a silicon photoanode with a titanium dioxide protective layer fabricated via atomic layer deposition using a first precursor tetrakis(dimethylamido)titanium(IV) and second precursor water at growth temperature 200 °C. A post-deposition heat treatment was performed during which an interfacial silicon dioxide layer forms to the detriment of the cell. Utilizing X-ray photoelectron spectroscopy and the Beer-Lambert law, the silicon dioxide interfacial layer can be analyzed. The heat treatment temperatures of 250, 300, and 500 °C resulted in a silicon dioxide layer of 1.3, 1.4, and 2.7 nm respectively while the sample that did not undergo a heat treatment had a silicon dioxide thickness of 0.3 nm. To investigate the impact of these results, stability and linear sweep voltammetry tests were carried out in an experimental photoelectrochemical cell with an alkaline aqueous solution (1 M NaOH, pH 13.6). From these tests, it is concluded that the silicon dioxide interfacial layer negatively impacts the performance of the cell but the higher heat treatment temperature results in an advantageous crystal structure. This was seen in the crystalline samples' ability to produce higher current densities over time and with increasing voltage.

Keywords: photoelectrochemical cell, X-ray photoelectron spectroscopy, atomic layer deposition, silicon, silicon dioxide, titanium dioxide, heat treatment

PREFACE

This thesis was completed as part of the Surface Science research group at Tampere University. While the global pandemic inhibited my ability to go the Surface Science laboratory in person, I was able to complete two research trainings and this thesis under the Surface Science research group's supervision. My motivation for completing this thesis comes from my belief that the development of clean, renewable energy is a worthy pursuit that only stands to globally benefit society economically, environmentally, and more. I have had the fortunate opportunity to have Professor Mika Valden and Dr. Jesse Saari as my supervisors for my research trainings and this thesis. I would like to extend my personal thanks to Dr. Jesse Saari, who has gone above and beyond in his gracious guidance of the creation of this thesis even after the start of his career away from Tampere University. The members of the science and engineering program, the members of TaSciEn, my close friends, and my family have all supported me in the production of this thesis. Without them, this thesis would not have been possible, and for that I have the utmost gratitude.

Tampere, 26th April 2023

Jadon Stuart

CONTENTS

LIST OF SYMBOLS AND ABBREVIATIONS

ALD	Atomic Layer Deposition
BE	Binding Energy
CB	Conduction Band
GIXRD	Grazing Incidence X-ray Diffraction
HER	Hydrogen Evolution Reaction
IMFP	Inelastic Mean Free Path
KE	Kinetic Energy
LSV	Linear Sweep Voltammetry
OER	Oxygen Evolution Reaction
PEC	Photoelectrochemical
STH	Solar-to-Hydrogen
TDMAT	tetrakis(dimethylamido)titanium(IV)
VB	Valence Band
XPS	X-ray Photoelectron Spectroscopy

1. INTRODUCTION

At the time of the writing of this thesis, an incalculable amount of research is being carried out in the hopes of developing clean, renewable energy production. This is deemed by many to be the holy grail of energy production and has implications for societal development that are barely understood.

Hydrogen is well-known for the fact that it only produces heat and water when it burns. Currently, a common source of hydrogen is from natural gas reforming [1]. Besides difficulties in cleanly collecting hydrogen, another primary issue is the infrastructure and technologies needed to use hydrogen as a fuel source. Infrastructure issues aside, if hydrogen was available in abundance at low economical and environmental cost this could revolutionize global energy production.

Following Edmond Becquerel's demonstration of the photovoltaic effect in 1839, scientists have been striving to implement technology to take advantage of this effect in renewable fuel production [2]. Photoelectrochemical (PEC) cells are one such technology designed to solve the problem of clean hydrogen production. Fujishima and Honda utilized a semiconductor electrode to achieve electrochemical water photolysis [3] in the 1970s. Unfortunately, modern PEC cells are not anywhere near the efficiency and low cost levels to be applied at large scale. The solar-to-hydrogen (STH) efficiency of PEC cells are currently only around a few percent. For example, with an alternative semiconductor (InGaP/GaAs double junction) Varadhan et al. was able to achieve a STH efficiency of 9 percent which is a notably higher STH efficiency than other attempts [4].

This thesis investigates PEC cells with a silicon semiconductor photoanode and a titanium dioxide (TiO_2) protective layer. The TiO_2 layer is formed via atomic layer deposition (ALD). The main variable analyzed in this thesis is the post-deposition heat treatment. Annealing TiO_2 is beneficial for developing crystallized TiO_2 [5]. Crystalline TiO_2 is more stable in an alkaline electrolyte environment which is necessary to efficiently drive the hydrogen production [6]. However, other research has also employed amorphous TiO_2 as a protective layer, though in the referenced case by Chen et al. a catalyst was also used which should increase the efficiency of the PEC cell [7]. This is to highlight the fact that developing a photoelectrode for a PEC cell is an extremely complex problem that requires a deep understanding of material science and related nuanced chemical and

physical principles.

It has been observed that the post-deposition heat treatment causes the development of an interfacial silicon dioxide (SiO_2) layer. SiO_2 is a well-known insulator, thus it is detrimental to the performance of the PEC cell [8]. Scheuermann et al. provide motivation to continue working on this problem as they demonstrated that the performance of the photoanode could be dramatically improved by fabricating a TiO_2/Si electrode with an SiO_2 interface that is less than 1 nm thick [9].

This thesis examines the effect of the heat treatment on the interfacial SiO_2 layer and crystallinity of the TiO_2 layer which both in turn effect the performance of the PEC cell. There are four main sections following this introduction chapter. First, the theoretical background chapter where the working principles of the PEC cell are described and the fundamentals of XPS are explained. The approximations and equations for calculating the interfacial SiO_2 layer are presented. Second, the methodology sections contains the experimental details regarding the ALD, heat treatment, XPS, and PEC cell set ups. Third, the results of the XPS analysis and PEC cell tests are given. Finally, the work is concluded with final thoughts regarding the experimental results and suggestions for further research.

2. THEORETICAL BACKGROUND

2.1 Photoelectrochemical Cell

As aforementioned, a PEC cell is a device that converts sunlight into electrical energy for the purpose of causing a water splitting reaction or to develop more complex hydrocarbon fuels [10]. The scope of this thesis only covers PEC cells that carry out water splitting reactions for hydrogen production. Within a PEC cell are one or two photoelectrodes submerged in an electrolyte. There is a large variety of PEC cell designs. The main factors that change are the amount of photoelectrodes (one or two), the electrolyte, the presence of a membrane separating the anode and cathode environment, and the materials used to fabricate the electrodes and their protective layer or catalysts [11]. In a research environment, a third electrode called the reference electrode is used for different tests such as setting and analyzing voltage values with reference to the hydrogen splitting potential.

This section outlines some of the basic physical and chemical properties required to understand the operation of a PEC cell. When a photon strikes a photoactive semiconductor, an electron moves from the valence band to the conduction band [10]. This electron is carried to the other electrode either via an external potential or an internal potential [10]. The holes/electrons on the surface of the electrodes react with the water to produce hydrogen and oxygen gas [10]. There may be two different electrolytes separated by a membrane that are favorable to creating hydrogen and oxygen gas [10]. An example diagram of a basic PEC cell is shown in Figure 2.1, however many variants are possible [10].

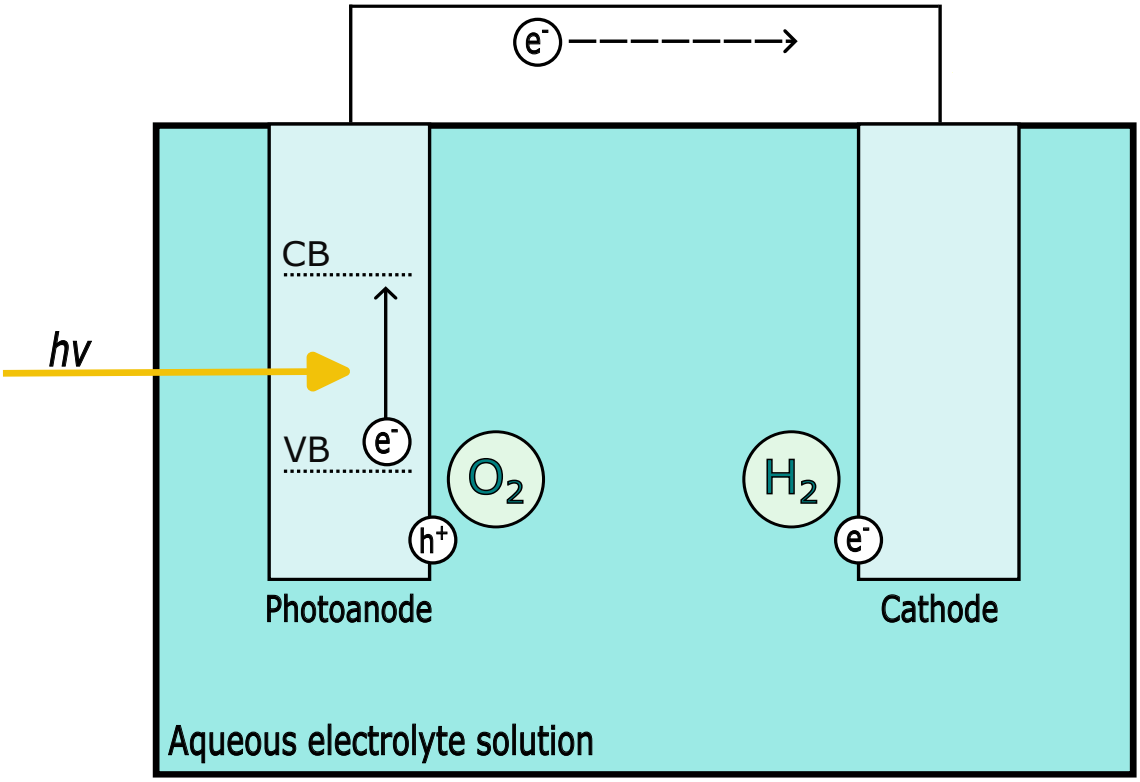

Figure 2.1. *PEC cell simple design. VB and CB stand for valence band and conduction band respectively. A photon excites an electron from the VB to the CB in the semiconductor of the photoanode (in this thesis, silicon). CB electrons flow from the photoanode to the cathode via an external circuit. At the surface of the anode, electron holes interact with water to produce oxygen [10]. At the surface of the cathode, electrons interact with water to produce hydrogen [10].*

We first turn our focus to how water splitting takes place as optimizing the water splitting reaction is the over-arching goal of a PEC cell. Water splitting is the following reaction [10].

$$2\mathrm{H_2O} \rightarrow 2\mathrm{H_2}(\mathrm{g}) + \mathrm{O_2}(\mathrm{g}) \tag{2.1}$$

This reaction can be split into the two half reactions, the hydrogen evolution reaction (HER) and the oxygen evolution reaction (OER). At the cathode, the HER occurs and water is reduced. At the anode, the OER occurs and water is oxidized [12]. To optimize the water splitting reaction, understanding the concept of the onset potential becomes crucial. The onset potential is defined as the lowest voltage value for which the OER will take place within preset conditions [13].

The lowest theoretical value for the OER is 1.23 V [10]. However, overpotentials are additional potentials required to drive the reaction efficiently. There are three overpotentials which are related to the HER, OER, and the ionic condition of the electrolyte. The following equation simply is the sum of the potentials that contribute to the onset potential for

water splitting to take place. Considering standard conditions, an electrolyte with an ionic concentration of 1 molar, ambient pressure of 1 atm, and ambient temperature of 298 K, the minimum voltage for water splitting in PEC cell is the following [10].

$$V_{\min}(j) = 1.23\text{eV} + \eta_{\text{HER}}(j) + \eta_{\text{OER}}(j) + \eta_{\text{ionic cond.}}(j) \tag{2.2}$$

This work investigates the operation of the photoanode. Previous work on PEC cells has found that optimizing the photoanode's performance is more difficult in comparison to the (photo)cathode [14].

Another vital detail to a well-operating PEC cell is the current density of the electrodes. An appropriately high current density ensures more efficient reactions, however the current density should not be too high to increase the overpotentials [10]. Important factors of the PEC cell's effective operation are that the current density is stable over time and that the photoelectrode remains intact without suffering corrosion [7]. One can measure the current density as a function of the potential relative to the reference electrode in hopes of seeing higher current density values for lower voltage values. Checking that the current density is stable over time is one way of investigating if the photoelectrode is intact. Visual examinations can easily be done - it can often be clearly seen by color change if corrosion has occurred.

2.2 TiO_2 Protection Layer for Photoelectrode

A protection layer is necessary for the electrodes in a PEC cell due to the aqueous electrolyte conditions. The aqueous electrolyte conditions can be acidic or alkaline and are corrosive to the electrodes [10]. This thesis deals with alkaline aqueous electrolyte conditions. TiO_2 is a well known protection layer for photoelectrodes and is in abundant supply and is easy to fabricate [10]. TiO_2 is a good protection layer because of its ability to transmit charge and stability [10]. These factors make it a great candidate for much research surrounding PEC cells [10].

Atomic layer deposition, a form of chemical vapor deposition, is the method of choice for depositing the TiO_2 layer for this work. When the TiO_2 is deposited it is amorphous. Annealing the TiO_2/Si becomes necessary to achieve a functional level of stability and protection [6]. TiO_2 generally forms into three crystal structures: anatase, brookite, and rutile. This thesis touches on the brookite-rutile and rutile phase which are formed from the annealing process.

During the annealing process a SiO_2 layer may form between the silicon and TiO_2 layers. This SiO_2 layer is an insulator and thus is detrimental to the performance of the PEC cell [8]. This trade-off between annealing the TiO_2/Si photoelectrode, thereby crystallizing the

TiO_2, and the formation of the SiO_2 layer forms the crux of this thesis. We will examine three types of heat treatment in comparison to the sample that does not receive heat treatment. To analyze the SiO_2 layer we employ X-ray photoelectron spectroscopy (XPS).

2.3 X-Ray Photoelectron Spectroscopy

XPS is a sensitive surface analysis technique for which many important details related to a solid surface are revealed. XPS is generally used for compositional analysis however we utilize XPS for morphological analysis. The typical range of analysis depth is approximately 10 nm and all elements except hydrogen and helium can be detected at atomic concentrations above 0.1% [15]. XPS is incredibly useful for analyzing the interface between TiO_2 and silicon in a PEC cell.

To understand the foundations of XPS, we first consider the interaction between an X-ray beam and the atom it strikes. The relevant scenario is when all of the X-ray photon energy is imparted into an orbiting electron of an atom and this photoelectron is emitted from the atom [15]. An imperative observation of this photoemission is that the intensity of the incident light is proportional to the number of photoelectrons [15]. Another crucial fact is that the frequency of the incoming photons is proportional to the kinetic energy of the photoelectrons [15].

With XPS we know the energy of the electron source (hv) and measure the kinetic energy (KE) of the photoelectron as shown by the following equation [15]. The binding energy (E_B) is of upmost importance because this is the value by which we can uniquely identify every element [15].

$$E_{\mathrm{B}} = hv - \mathrm{KE} \tag{2.3}$$

The end result we are searching for is the thickness of layers of our sample. The Beer-Lambert law provides the basis for finding this result [15].

$$I = I_0 \, e^{-d/\lambda} \tag{2.4}$$

In the above equation, I_0 is the intensity of the photoelectron, λ is the inelastic mean free path (IMFP), d is the distance into the material, and I is the intensity after exiting the material. As an electron moves in a medium with a certain energy, it collides with the medium. The average distance between these collisions is the IMFP [16]. XPS data helps us model the morphology of our sample, yielding a relationship between intensity and binding energy. This allows us to identify an element and calculate its thickness.

Another powerful feature of XPS is that we can calculate the concentration of each el-

ement in our sample. While this is not the focus of this thesis, it is extremely relevant background for XPS. The area under the peak of data helps us find the concentration of each element [15].

$$I_{ij} = KT(\mathrm{KE})L_{ij}(\gamma)\sigma_{ij}\int n_i(z)\mathrm{e}^{-z/\lambda(\mathrm{KE})\cos\theta}\mathrm{dz} \tag{2.5}$$

As succinctly encapsulated in Surface Analysis: The Principle Techniques, "I_{ij} is the area of peak j from element i, K is an instrumental constant, $T(KE)$ is the transmission function of the analyzer, $L_{ij}(\gamma)$ is the angular asymmetry factor for orbital j of element i, σ_{ij} is the photoionization cross-section of peak j from element i, $n_i(z)$ is the concentration of element i at a distance z below the surface, $\lambda(KE)$ is the inelastic mean free path length, and θ is the take-off angle of the photoelectrons measured with respect to the surface normal [15]." Surface Analysis: The Principle Techniques by Vickerman and Gilmore was the primary source used to understand the background of XPS [15]. XPS provides the necessary data to calculate the SiO_2 thickness in our sample.

2.3.1 Calculating Interfacial SiO_2 Thickness

As we have the means to produce and investigate a PEC cell, we should consider how to optimize our PEC cell. Ros et al. propose six primary phenomena which must be optimized for a well-designed PEC cell. The most relevant point mentioned is maximizing the charge separation and transport considering we are dealing with a multi-layered semiconductor [10]. To determine how the SiO_2 layer affects the performance of our PEC cell we need to know the thickness of the SiO_2 layer.

Newberg et al. provides the necessary equations to calculate the thickness of the SiO_2 layer based on the Beer-Lambert law [17]. Considering a film of thickness t_f and using the straight-line approximation, we can calculate the photoelectron's intensity I_f after having passed through a layer of a given material f [17]. In the following equations, S is the photoemission spectroscopy constant, j is the inner shell orbital, and λ' is the inelastic mean free path (IMFP) normalized to the sample [17].

$$I_f = S_f^j \int_0^{t_f} e^{-z/\lambda'_f} dz = S_f^j \lambda'_f \left(1 - e^{-t_f/\lambda'_f}\right) \tag{2.6}$$

Utilizing the final part of the equation, we write the equation for the intensity of the TiO_2 layer.

$$I_{\mathrm{TiO_2}} = S_{\mathrm{TiO_2}}^{\mathrm{Ti2p}} \lambda_{\mathrm{TiO_2}}^{\mathrm{Ti2p}} \left[1 - \exp\left(-t_{\mathrm{TiO_2}}/\lambda_{\mathrm{TiO_2}}^{\mathrm{Ti2p}}\right)\right] \tag{2.7}$$

In XPS analysis we focus on the most intensive peaks which are easier to identify. In the case for silicon, the 2p electron peak is easiest to identify. We then write the intensity of the photoelectrons having passed through the SiO_2 layer. The final term is to account for the photoelectrons having passed through the TiO_2 layer. We analyze the photoelectrons that do not lose any kinetic energy when passing through the SiO_2 layer and the TiO_2 layer. Many photoelectrons lose their energy and will not form the characteristic peak in the XPS spectrum.

$$I_{\mathrm{SiO_2}} = S_{\mathrm{SiO_2}}^{\mathrm{Si4+2p}} \lambda_{\mathrm{SiO_2}}^{\mathrm{Si4+2p}} \left[1 - \exp\left(-t_{\mathrm{SiO_2}}/\lambda_{\mathrm{SiO_2}}^{\mathrm{Si4+2p}}\right)\right] \left[\exp\left(-t_{\mathrm{TiO_2}}/\lambda_{\mathrm{TiO_2}}^{\mathrm{Si4+2p}}\right)\right] \tag{2.8}$$

We then write the intensity of the photoelectrons having originated from the silicon substrate. The final term is to account for the photoelectrons having passed through the TiO_2 and SiO_2 layers.

$$I_{\mathrm{Si}} = S_{\mathrm{Si}}^{\mathrm{Si2p}} \lambda_{\mathrm{Si}}^{\mathrm{Si2p}} \left[\exp\left(-t_{\mathrm{SiO_2}}/\lambda_{\mathrm{SiO_2}}^{\mathrm{Si2p}}\right)\right] \left[\exp\left(-t_{\mathrm{TiO_2}}/\lambda_{\mathrm{TiO_2}}^{\mathrm{Si2p}}\right)\right] \tag{2.9}$$

We can solve for the thickness of the SiO_2 layer by taking the ratio of equation 2.9 to equation 2.8 and rearranging.

$$t_{\mathrm{SiO_2}} = \lambda_{\mathrm{SiO_2}}^{\mathrm{Si2p}} \ln\left[1 + \frac{I_{\mathrm{SiO_2}}}{I_{\mathrm{Si}}} \frac{N_{\mathrm{Si}} \lambda_{\mathrm{Si}}^{\mathrm{Si2p}}}{N_{\mathrm{SiO_2}} \lambda_{\mathrm{SiO_2}}^{\mathrm{Si2p}}}\right] \tag{2.10}$$

N, the number of atoms per unit volume, arises from taking the ratio $\mathrm{S}_{\mathrm{Si}}^{\mathrm{Si2p}}/\mathrm{S}_{\mathrm{SiO_2}}^{\mathrm{Si4+2p}}$ as all other factors in this ratio cancel out except for N. Further detailing of the photoemission spectroscopy constant is not necessary in our case as we are strictly concerned with the thickness of the SiO_2 layer. We also approximate $\lambda_{\mathrm{SiO_2}}^{\mathrm{Si2p}} = \lambda_{\mathrm{SiO_2}}^{\mathrm{Si4+2p}}$. This causes the last terms in equations 2.8 and 2.9 to cancel out when taking the ratio $I_{\mathrm{Si}}/I_{\mathrm{SiO_2}}$. We can make this approximation as the photoelectron kinetic energy difference between Si and SiO_2 is minimal. The intensities are provided by the XPS measurements. Equations 2.7–2.10 were provided by Saari et al. [6].

3. METHODOLOGY

This section describes the methodologies, instruments, and specifications used in this work. The instrumentation and processes necessary to understand the basics of ALD and XPS are explained with the inclusion of relevant experimental values. The details of the PEC cell experiment are also described thoroughly.

An important note is that the XPS analysis is performed on samples of 2 nm TiO_2. However, the PEC cell experiment was done with a TiO_2 layer of 30 nm. The reason for this discrepancy is because of the nature of XPS analysis which cannot take measurements of samples with a depth as large as 30 nm. Hence it would be impossible to investigate the SiO_2 layer. It is assumed that the SiO_2 layer affects the 2 nm and 30 nm samples the same so the results can be linked. More discussion regarding this is in the conclusions section of this thesis.

3.1 Atomic Layer Deposition

ALD is a chemical vapor deposition method used to fabricate the protective layer on the silicon substrate. This ALD was carried out in a four step cycle. First, tetrakis(dimethylamido)titanium(IV) was released into the reaction chamber for 1.6 seconds. Second, there was a purge of argon for 6 seconds. Third, ultrapure water was released for 0.1 seconds. Finally, the reaction chamber was purged again with argon for 6 seconds. The ideally deposited thickness of TiO_2 is dependent on the number of cycles. In this case it was found that 58 cycles were needed for 2 nm of TiO_2 and 870 cycles were needed for 30 nm of TiO_2.

More details of the ALD process is listed in the table below. All of the TiO_2 films were deposited with the same method.

Table 3.1. *ALD experimental details.*

ALD reactor:	Picosun Sunale ALD R-200 Advanced
Substrates:	n-type Si(100)
Substrate/growth temperature:	200 °C
Carrier gas:	Argon (99.9999%)
1st precursor:	TDMAT (tetrakis(dimethylamido)titanium(IV))
1st precursor temperature:	76 °C
2nd precursor:	Ultrapure Milli-Q H_2O
2nd precursor temperature:	18 °C
ALD cycle (1st/purge/2nd/purge):	1.6s/6.0s/0.1s/6.0s
Number of ALD cycles:	58 cycles (2 nm)

3.2 Heat Treatment

Each sample went through a heat treatment with the goal of forming crystallized TiO_2. Four of the same depositions were performed, three of which went through an annealing process. This thesis uses the terms heat treatment and annealing interchangeably. The annealing was performed in a heated tube furnace in ambient air. The samples cooled down for a long period of time.

Table 3.2. *Post-deposition heat treatment temperatures and duration of TiO_2/Si samples.*

Heat treatment temperature (°C)	Duration (hours)
250 °C	10
300 °C	1
500 °C	1

In previous tests, it was observed that a heat treatment for 1 hour at 250 °C is not enough to fully crystallize the surface. At 300 °C it was found that 1 hour is long enough to crystallize the surface. Saari et al. provide good work and explanation for the relation between the time and temperature of annealing [18].

3.3 X-ray Photoelectron Spectroscopy

As aforementioned, we utilize XPS for morphological analysis in this thesis. An ultrahigh vacuum is required for XPS to be performed which was obtained with multiple types of

vacuum and pump technologies (scroll pump, turbo pump, and ion pump). A notable property of the XPS arrangement is the characteristic Al Kα peak of 1486.5 eV originating from the aluminum anode of the X-ray source. The following table summarizes the specifications used in the XPS and interfacial SiO_2 thickness analysis. Notable constants are listed that are used in later calculations.

Table 3.3. *XPS experimental details and related constants.*

XPS system:	ESCA3000
Excitation source:	Al Kα (1486.5 eV)
IMFP of Si 2p electrons in Si [6]	3.09 nm
IMFP of Si 2p electrons in SiO_2 [6]	3.75 nm
The number of Si atoms in Si per nm^3 [6]	49.737 $1/nm^3$
The number of Si atoms in SiO_2 per nm^3 [6]	26.557 $1/nm^3$

The data obtained from XPS measurements is binding energy (eV) and the corresponding intensity of the photoelectrons (counts/second). The phases of TiO_2 were determined by grazing incidence X-ray diffraction (GIXRD). Calculations to determine the Si and SiO_2 intensities were done with CasaXPS.

3.4 PEC Cell Specifications

The PEC cell in this experiment had a platinum cathode and a silver/silver chloride reference electrode. The ALD TiO_2/Si photoanode was the tested sample. Voltage was held constant (at 1.23 V) with Autolab PGSTAT12 potentiostat (Metrohm AG). The aqueous solution electrolyte was 1 M NaOH (pH 13.6). The solar spectrum was simulated with a HAL-C100 solar simulator (Asahi Spectra Co., Ltd., JIS Class A at 400–1100 nm with AM1.5G filter). An intensity of 1.00 Sun was verified with a 1 sun checker (model CS-30, Asahi Spectra Co., Ltd.).

4. RESULTS AND ANALYSIS

This section outlines the key findings of this thesis primarily in two major ways. We begin by investigating the XPS data which yields the SiO_2 thickness. We then turn our attention to the performance and stability of the PEC cell.

Different phases of TiO_2 have different electrical properties. The most essential differences between the phases of TiO_2 is that the higher the level of crystallinity of the TiO_2, the better protection and electrical properties it has [6]. Thus, the first notable data presented is the phase of TiO_2 formed after exposure to certain temperatures.

Listed in the table below are the phases of TiO_2 thin films after ALD deposition and the post-deposition annealing at 250 °C, 300 °C, and 500 °C. As dep refers to the sample that received no post-deposition heat treatment. These are the 30 nm TiO_2 samples that were used in the PEC cell experiment. It is advantageous to gather as much data as possible about the samples actually used in the PEC cell experiment, therefore we report the phases of TiO_2 for these samples and not the 2 nm TiO_2 samples. We refer to the 2 nm TiO_2 samples as TiO_2(2 nm)/SiO_2/Si and the 30 nm TiO_2 samples as TiO_2(2 nm)/SiO_2/Si, now including the SiO_2 layer.

Table 4.1. *Phases of TiO_2 of TiO_2(30 nm)/SiO_2/Si samples after post-deposition heat treatment.*

TiO_2(30 nm)/SiO_2/Si samples (heat treatment temperature)	TiO_2(30 nm) phases
As dep	Amorphous
250 °C	Rutile–Brookite mixed phase
300 °C	Rutile–Brookite mixed phase
500 °C	Rutile

As will be observed in other results, the 250 °C and 300 °C samples behave similarly which can be attributed to their same phase of TiO_2. Evidently higher annealing temperatures yield a more crystalline TiO_2 structure.

4.1 XPS Analysis and SiO_2 Thickness

This section contains the XPS results and Beer-Lambert Law analysis. The XPS graphs for each sample are overlaid so that one notices the difference of the size in the peaks, especially at 103 eV. The lines at 99.5 and 103 eV are the Si 2p peak binding energy values for metallic Si and SiO_2, respectively.

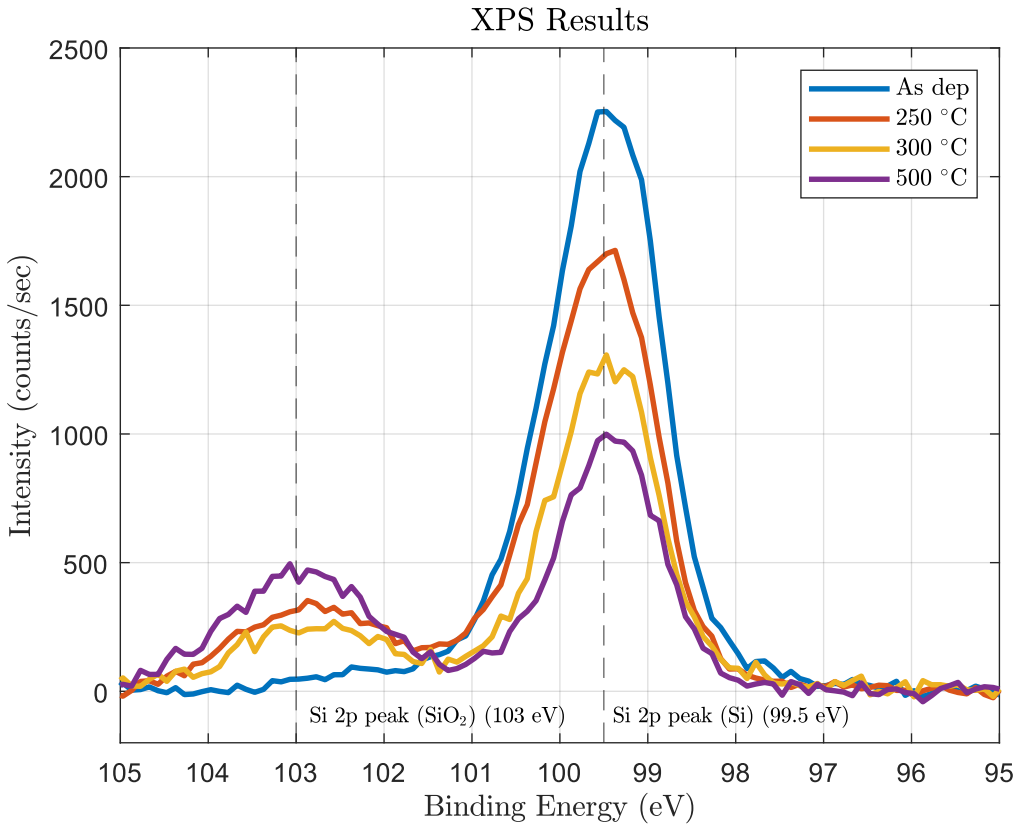

Figure 4.1. *XPS results for three TiO_2(2 nm)/SiO_2/Si samples post-annealing and one sample receiving no heat treatment. The two visible peaks at 103 eV and 99.5 eV are the Si 2p peak for SiO_2 and Si, respectively. Morphological analysis calculations are based on the area of these two peaks.*

As the heat treatment temperature increases, we notice the ratio of the intensities SiO_2/Si increases. We notice this implies an increase of the amount of SiO_2. The table below shows the relative concentrations of metallic Si and SiO_2 extracted from the XPS data, confirming this statement.

Table 4.2. *Si and SiO_2 relative intensities.*

	Si 2p (Si)	Si4+ 2p (SiO_2)
As dep	95.59	4.41
250 °C	78.42	21.57
300 °C	77.08	22.92
500 °C	59.33	40.68

Table 4.2 provides the I_{Si} and $I_{\mathrm{SiO_2}}$ values needed in equation 2.10. The other values we utilize from the methodology section are the IMFP values of 3.09 nm and 3.75 nm for Si 2p electrons through Si and SiO_2, respectively, and the atomic density (atoms/cubic nanometer) of 49.737 and 26.557 for Si and SiO_2 respectively. These are all the necessary values to find the SiO_2 thickness.

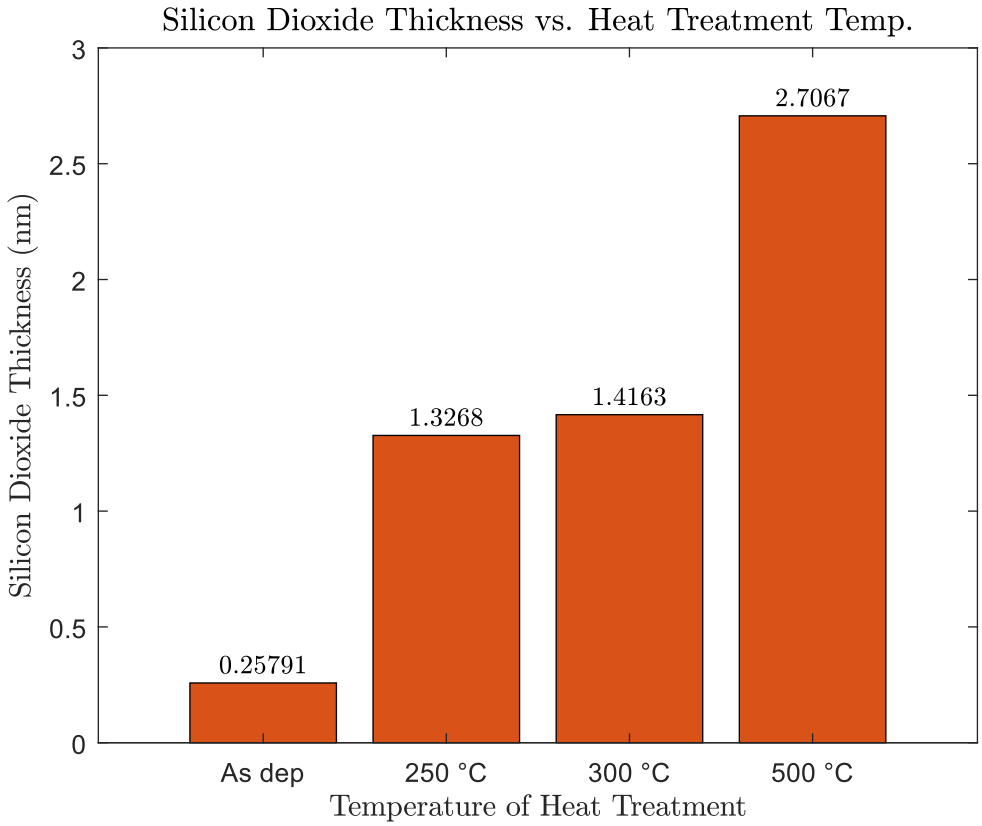

Figure 4.2. *Interfacial SiO_2 thickness in TiO_2(2 nm)/SiO_2/Si samples after ALD (as dep) and after heat treatment at 250 °C (10 h), 300 °C (1 h), and 500 °C (1 h). Calculated based on the XPS results and Beer-Lambert law.*

Figure 4.2 clearly shows that increased annealing temperatures is correlated with the formation of more SiO_2 which was expected. The values are comparable to the results found by Saari et al. [6].

We now turn our attention to how the SiO_2 affects the performance of the PEC cell.

4.2 Onset Potential

We are greatly interested in the onset potential of the PEC cell. In a linear sweep voltammetry (LSV) test, we can plot voltage values against the current density of our sample. This is done under simulated sunlight (1 sun) as well as in the dark. The purpose of the dark test is to confirm that the simulated sunlight generates photocurrent in the PEC cell. If the dark test does not produce zero values for the current density, there is a problem somewhere (likely that the TiO_2 coating dissolved).

1.23 volts is plotted on Figure 4.3 and Figure 4.4 to make clear where the potential required to obtain water splitting.

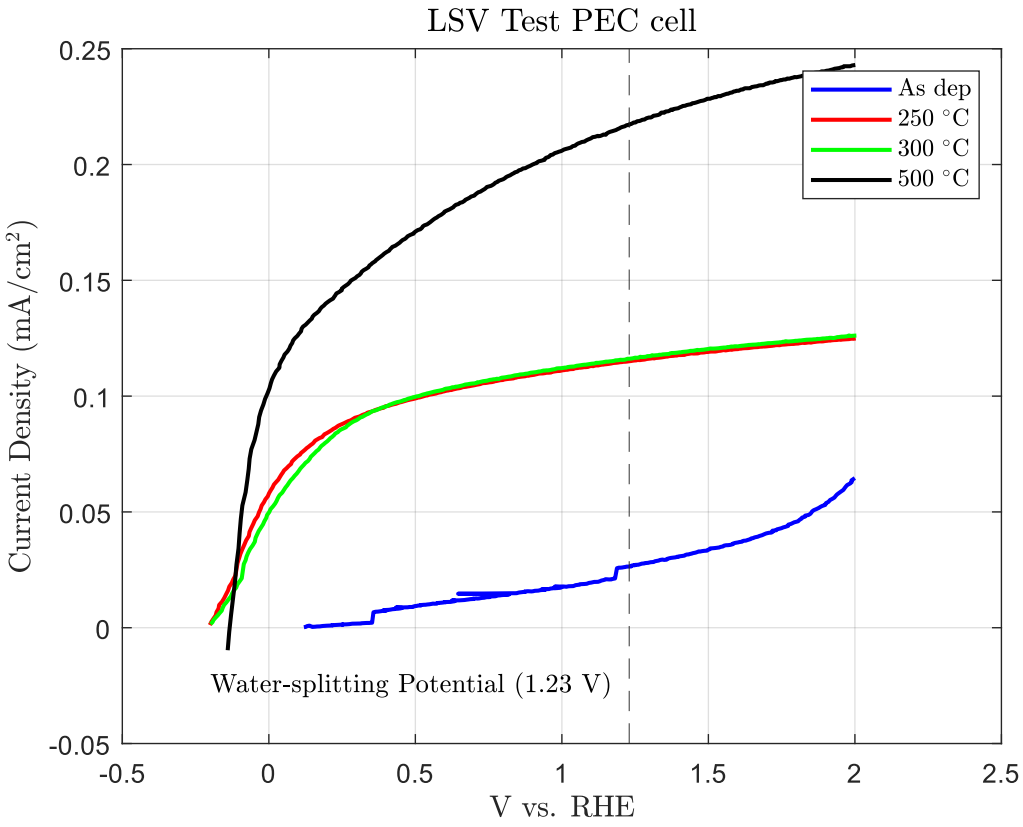

Figure 4.3. *LSV test under 1 sun for TiO_2(30 nm)/SiO_2/Si samples.*

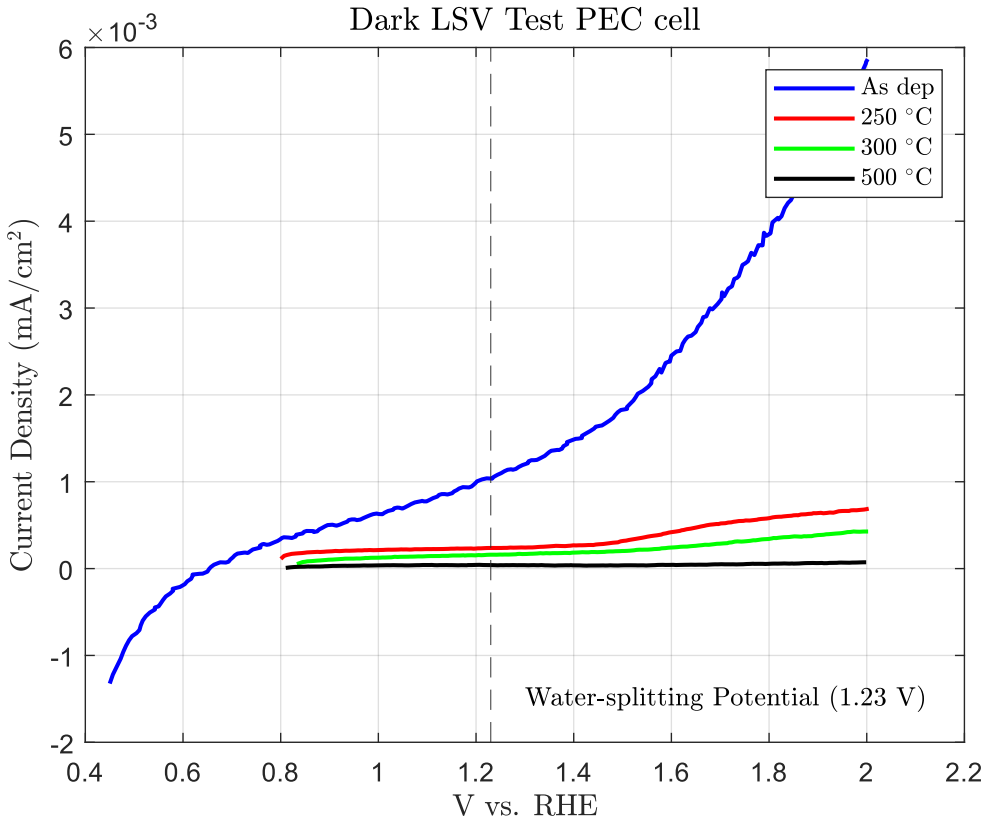

Figure 4.4. *LSV test in darkness for TiO_2(30 nm)/SiO_2/Si samples.*

There are two main results to dissect from Figure 4.3. Firstly, the 500 °C sample reached highest current density values. This can be explained by better electrical properties (less crystal defects) or because the crystalline rutile TiO_2 is a better catalyst material. It is quite difficult to say with any certainty if these reasons are valid without further testing. Secondly, the 250 °C and 300 °C samples both reached the lowest onset potential values. This can be explained because of a thinner interfacial SiO_2 layer. However, the overall photocurrent slopes are lower than the 500 °C sample so it is difficult to say which one is better. While the 250 °C and 300 °C samples had lower onset potential values, the drawback of lower current density values is concerning as this will limit the rate of the water splitting reaction. Generally the crystalline samples did well in the stability tests especially when compared to the amorphous sample which did not do well.

The dark LSV test yielded results that matched the theory that the rutile-brookite and rutile samples are more stable than the amorphous sample. The crystalline samples showed no dark current, while the amorphous sample did. In regards to the amorphous sample, this could possibly be explained by the degradation of the TiO_2 or silicon layer. The degraded protection could cause unexpected current flow, as well as other mechanisms that are out of the scope of this thesis.

4.3 PEC Stability

Two different stability tests were performed - a chopped light test and a 24 hour test (the end of which was the chopped light test). The results of these tests are shown below in Figure 4.5 and Figure 4.6.

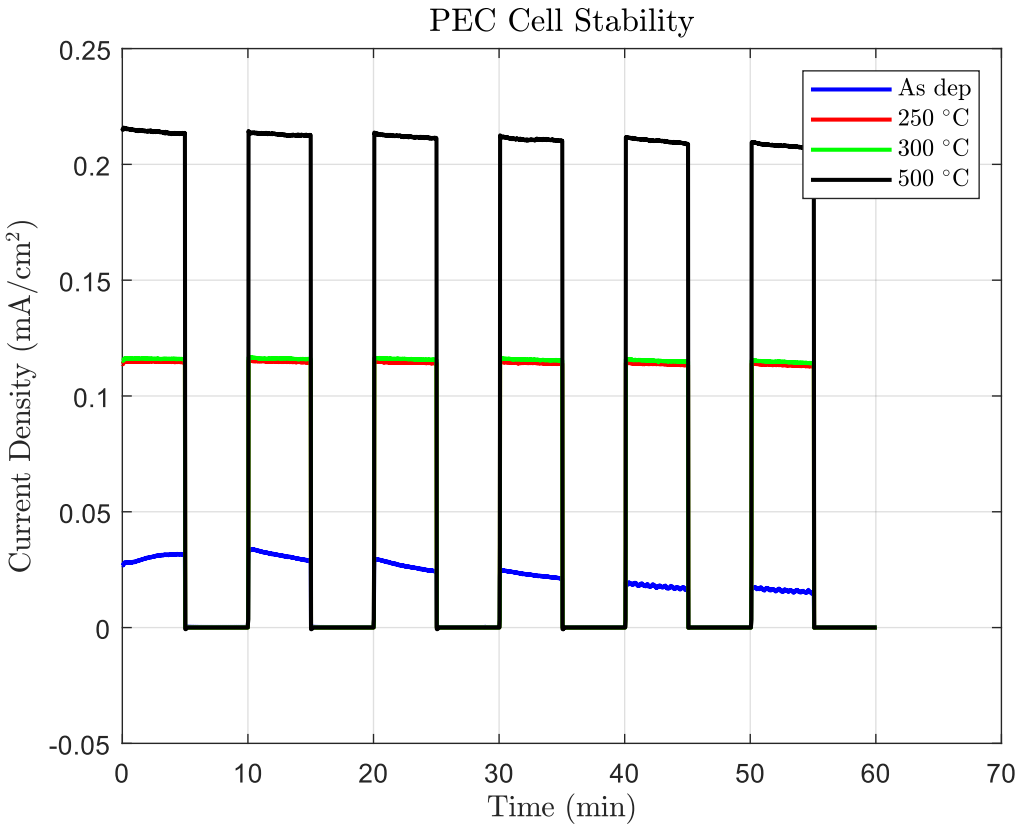

Figure 4.5. *PEC cell stability over one hour via chopped light test for TiO_2(30 nm)/SiO_2/Si samples. The sample receiving no heat treatment noticeably under-performs compared to the annealed samples.*

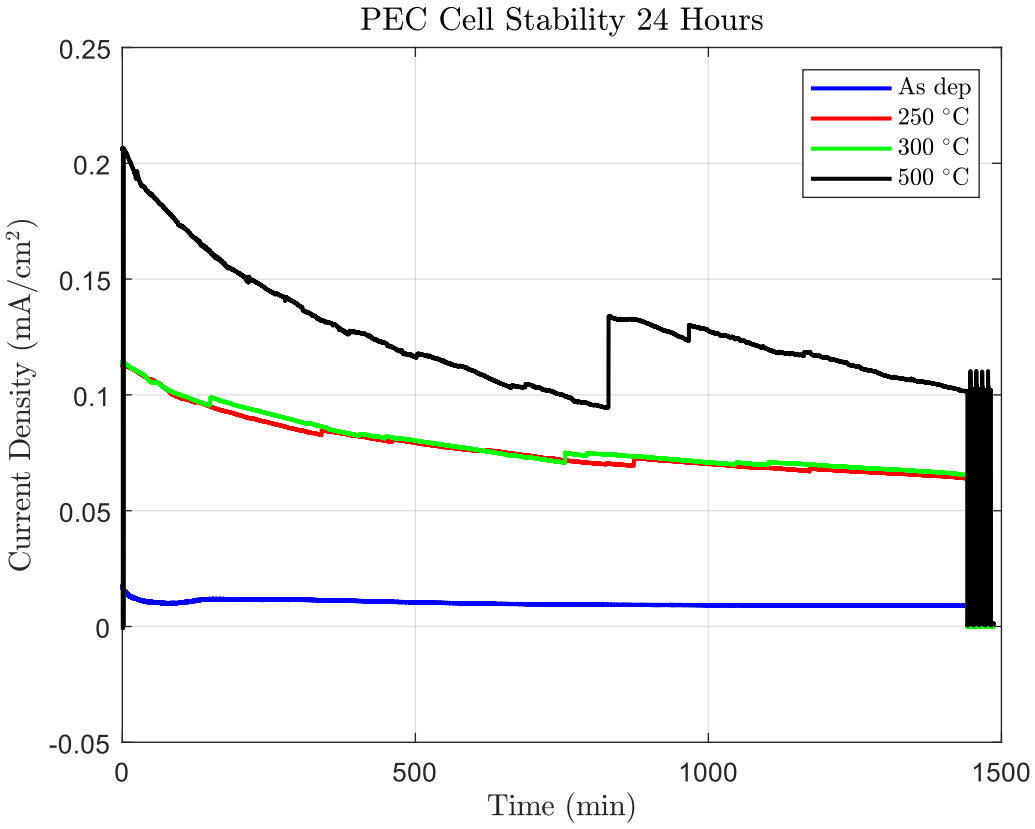

Figure 4.6. *PEC cell stability over 24 hours (chopped light test at end) for TiO_2(30 nm)/SiO_2/Si samples. Anomaly around 800 minute mark for 500 °C sample.*

The sample with the highest heat treatment temperature clearly showed the highest stability. The noticeably strange graph shape around minute 800 in the 24 hour light test could be attributed to a bubble popping and dramatically affecting the current density. However, there are many possible explanations for this abnormality.

Both of the stability tests once again confirm the similarity between the 250 °C and 300 °C samples. The stability tests demonstrate the advantage of a better crystal structure. In the chopped light test, the amorphous sample was clearly not producing a stable current over time. Even after a simple visual inspection, one can see evidence of degradation of the amorphous sample and not on the crystalline samples.

Ros et al. suggest that PEC cells have an operating current density in the tens of mA/cm^2 [10]. The LSV and stability tests do not produce values this high; the PEC cell in this thesis is designed for research and has not yet been optimized for efficient hydrogen production. Thus there is no analysis of how much oxygen or hydrogen was produced as this was not the aim of this thesis.

5. CONCLUSION

This thesis has investigated the effect of heat treatment on a silicon photoanode with a TiO_2 protective layer fabricated via ALD. After gathering data regarding the interfacial SiO_2 layer that developed during the heat treatment with XPS and Beer-Lambert law analysis, stability and LSV tests were performed on the PEC cell.

From this experiment, we gathered three main conclusions. First, interfacial SiO_2 seems to have a negative impact on the onset potential of photocurrent in the PEC cell as shown in Figure 4.3. However, the sample with the highest temperature heat treatment reached higher current density values. Second, increased crystalline structure of the TiO_2 outer layer seems to increase stability of photocurrent generation over time. Third, amorphous TiO_2, when compared to crystalline TiO_2, has less effective stability and photocurrent generation.

In response to the title of this thesis, we can say that the impact of the development of interfacial SiO_2 is not so detrimental that it outweighs the benefits of the heat treatment. The benefit of the TiO_2 protective layer having crystalline properties is so beneficial to the protection and stability of the PEC that it becomes necessary.

As aforementioned in the methodology of this thesis, the samples analyzed with XPS (2 nm TiO_2) were not the same as the samples used in the PEC cell performance tests (30 nm TiO_2). This is noted so that it is clear that the XPS and Beer-Lambert law analysis and the performance of the PEC cell are most likely but not definitely correlated. However, there has been no reason found why this yields results that are misleading or would not at least be indicative of the results that would be found otherwise.

Some recommendations for further research include four main topics. First, instead of using XPS to analyze the samples, other methods could be considered. This is due to the limitations of the depth of analysis of XPS. Another methodology for thin film analysis is cross-sectional transmission electron spectroscopy which McDowell et al. use to also analyze SiO_2 thickness [19]. Second, other recipes for the ALD can be considered. ALD is a delicate process and may have notably different results based on the precursors, temperatures, and purge cycle used. Third, other materials for the semiconductors and protective layers should be considered when designing a PEC cell. Silicon and TiO_2 are very common selections, but other choices such as GaAs as aforementioned have also

yielded promising results. Finally, other designs for PEC cells should be researched. One primary factor not discussed in detail in this thesis that could be altered is the electrolyte so that the electrodes are not exposed to such corrosive environments.

This thesis has demonstrated evidence that the development of a SiO_2 interfacial layer is detrimental to the performance of a PEC cell. On the other hand, the benefits of crystalline TiO_2 have also been displayed with its success in the LSV and stability tests. Therefore, the benefits of a post-deposition heat treatment on a Si/TiO_2 photoanode for a PEC cell seem to outweigh the negative effects of the interfacial SiO_2.

REFERENCES

[1] *Hydrogen Production and Distribution*. URL: https://afdc.energy.gov/fuels/hydrogen_production.html.

[2] *First Photovoltaic Devices*. URL: https://web.archive.org/web/20100718084539/http://www.pveducation.org/pvcdrom/manufacturing/first-photovoltaic-devices.

[3] Fujishima, A. and Honda, K. Electrochemical Photolysis of Water at a Semiconductor Electrode. *Nature* (July 1972), pp. 37–38. DOI: 10.1038/238037a0.

[4] Varadhan, P., Fu, H.-C., Kao, Y.-C., Horng, R.-H. and He, J.-H. An efficient and stable photoelectrochemical system with 9% solar-to-hydrogen conversion efficiency via InGaP/GaAs double junction. *Nature Communications* (Nov. 2019), p. 5282. DOI: 10.1038/s41467-019-12977-x.

[5] Khan, R., Ali-Löytty, H., Saari, J., Valden, M., Tukiainen, A., Lahtonen, K. and Tkachenko, N. V. Optimization of Photogenerated Charge Carrier Lifetimes in ALD Grown TiO2 for Photonic Applications. *Nanomaterials* (2020). DOI: 10.3390/nano10081567.

[6] Saari, J., Ali-Löytty, H., Honkanen, M., Tukiainen, A., Lahtonen, K. and Valden, M. Interface Engineering of TiO2 Photoelectrode Coatings Grown by Atomic Layer Deposition on Silicon. *ACS Omega* (2021), pp. 27501–27509. DOI: 10.1021/acsomega.1c04478.

[7] Chen, Y. W., Prange, J. D., Dühnen, S., Park, Y., Gunji, M., Chidsey, C. E. D. and McIntyre, P. C. Atomic layer-deposited tunnel oxide stabilizes silicon photoanodes for water oxidation. *Nature Materials* (July 2011), pp. 539–544. DOI: 10.1038/nmat3047.

[8] Reed, M. L. and Fedder, G. K. 2 - Photolithographic Microfabrication. *Micro Mechanical Systems*. Ed. by T. Fukuda and W. Menz. Handbook of Sensors and Actuators. Elsevier Science B.V., 1998, pp. 13–61. DOI: https://doi.org/10.1016/S1386-2766(98)80003-0.

[9] Scheuermann, A. G., Kemp, K. W., Tang, K., Lu, D. Q., Satterthwaite, P. F., Ito, T., Chidsey, C. E. D. and McIntyre, P. C. Conductance and capacitance of bilayer protective oxides for silicon water splitting anodes. *Energy Environ. Sci.* (2016), pp. 504–516. DOI: 10.1039/C5EE02484F.

[10] Ros, C., Andreu, T. and Morante, J. R. Photoelectrochemical water splitting: a road from stable metal oxides to protected thin film solar cells. *J. Mater. Chem. A* (2020), pp. 10625–10669. DOI: 10.1039/D0TA02755C.

[11] Decker, F. and Cattarin, S. PHOTOELECTROCHEMICAL CELLS | Overview. *Encyclopedia of Electrochemical Power Sources*. Ed. by J. Garche. Amsterdam: Elsevier, 2009, pp. 1–9. DOI: https://doi.org/10.1016/B978-044452745-5.00035-6.

[12] Wang, S., Lu, A. and Zhong, C.-J. Hydrogen production from water electrolysis: role of catalysts. *Nano Convergence* 8 (Feb. 11, 2021), p. 4. DOI: 10.1186/s40580-021-00254-x.

[13] Sanchis-Gual, R., Seijas-Da Silva, A., Coronado-Puchau, M., Otero, T. F., Abellán, G. and Coronado, E. Improving the onset potential and Tafel slope determination of earth-abundant water oxidation electrocatalysts. *Electrochimica Acta* (2021), p. 138613. DOI: https://doi.org/10.1016/j.electacta.2021.138613.

[14] Cheng, C., Zhang, W., Chen, X., Peng, S. and Li, Y. Strategies for improving photoelectrochemical water splitting performance of Si-based electrodes. *Energy Science & Engineering* (2022), pp. 1526–1543. DOI: https://doi.org/10.1002/ese3.1087.

[15] Vickerman, J. C. and Gilmore, I. *Surface Analysis: The Principal Techniques*. 2. Aufl. New York: Wiley, 2009.

[16] Le, D.-N. and Nguyen-Truong, H. T. Analytical Formula for the Electron Inelastic Mean Free Path. *The Journal of Physical Chemistry C* (Sept. 2, 2021), pp. 18946–18951. DOI: 10.1021/acs.jpcc.1c05212.

[17] Newberg, J. T., Starr, D. E., Yamamoto, S., Kaya, S., Kendelewicz, T., Mysak, E. R., Porsgaard, S., Salmeron, M. B., Brown, G. E., Nilsson, A. and Bluhm, H. Formation of hydroxyl and water layers on MgO films studied with ambient pressure XPS. *Surface Science* (2011), pp. 89–94. DOI: https://doi.org/10.1016/j.susc.2010.10.004.

[18] Saari, J., Ali-Löytty, H., Lahtonen, K., Hannula, M., Palmolahti, L., Tukiainen, A. and Valden, M. Low-Temperature Route to Direct Amorphous to Rutile Crystallization of TiO2 Thin Films Grown by Atomic Layer Deposition. *The Journal of Physical Chemistry C* (2022), pp. 15357–15366. DOI: 10.1021/acs.jpcc.2c04905.

[19] McDowell, M. T., Lichterman, M. F., Carim, A. I., Liu, R., Hu, S., Brunschwig, B. S. and Lewis, N. S. The Influence of Structure and Processing on the Behavior of TiO2 Protective Layers for Stabilization of n-Si/TiO2/Ni Photoanodes for Water Oxidation. *ACS Applied Materials & Interfaces* (2015), pp. 15189–15199. DOI: 10.1021/acsami.5b00379.